Comparison of neutron-scattering data for tetrahedral amorphous carbon with structural models

K. W. R. Gilkes* and P. H. Gaskell
Cavendish Laboratory, Madingley Road, Cambridge CB3 0HE, United Kingdom

J. Robertson
Engineering Department, Trumpington Street, Cambridge CB2 1PZ, United Kingdom
(Received 6 September 1994)

Several physical models are compared with the experimental reduced radial distribution function $G(r)$ derived from high-resolution pulsed-neutron-scattering data for tetrahedral amorphous carbon. These models include tetrahedral models for amorphous silicon in addition to models constructed specifically to model high-density amorphous carbon. While the tetrahedral models provide better overall agreement than some amorphous carbon models containing threefold sites, no model provides an adequate level of agreement, particularly in the breadth of the first-neighbor distribution. The second-neighbor distribution of some of the models is found to be asymmetric, and this removes the inconsistency found between the measured first and second coordination numbers. Refinement of several models is attempted using a modified form of the reverse Monte Carlo algorithm, and some are successfully refined without topological alterations. For the tetrahedral models, introduction of pairs of threefold sites is found to produce structures in very good agreement with the experimental $G(r)$. The high levels of elastic strain in the best models suggests that a high strain energy is an essential property of tetrahedral amorphous carbon.

I. INTRODUCTION

There is considerable interest in the structure and properties of amorphous carbon (*a*-C), which can be prepared from a hydrocarbon plasma or from ion beams. Films deposited from a filtered ion beam or a laser plasma are found to possess very high density and hardness.[1–6] Recently, films grown using a filtered cathodic arc[5–11] were shown to possess a proportion of fourfold sites in excess of 80%.[7,8] These films have an optical gap of over 2 eV, and can be doped *n*-type with both N and P,[9–11] establishing the material as a technologically important amorphous semiconductor. An earlier neutron-scattering study suggested that its structure is a predominantly tetrahedral network.[12] This form of *a*-C has been denoted "tetrahedral amorphous carbon" (*ta*-C), to distinguish it structurally from other forms of *a*-C.

This highly tetrahedral *a*-C may be an important new structural form of C, namely the tetrahedrally bonded analog of *a*-Si (or *a*-Ge). It is therefore necessary to investigate the atomic structure of *ta*-C thoroughly, in order to determine the extent to which this analogy holds. Unlike *a*-Si, *ta*-C contains a significant fraction of threefold sites. However, these do not all behave as defects: π bonds tend to form with neighboring threefold sites to form pairs or larger π-bonded clusters, whereas in unhydrogenated *a*-Si the threefold sites remain isolated as dangling bonds. This difference has important consequences for electronic properties requiring doping, which is ineffective without hydrogenation of the material. In *ta*-C, however, the density of unpaired electrons is some two orders of magnitude lower than in *a*-Si,[10] perhaps due to the tendency of π states to pair and form states outside the gap.

The present work addresses the structural study of *ta*-C by comparing new, high-resolution neutron-diffraction data with existing structural models and by refining these models to give better agreement with experiment.

II. NEUTRON SCATTERING

An earlier neutron-scattering study of *ta*-C (Ref. 12) had limited resolution. The small specimen mass available at the time ($\approx$30 mg) forced a measurement at the highest neutron flux available (at a wavelength of 0.07 nm) with a maximum scattering vector of 163 nm^{-1}. The present study has been carried out on a much larger specimen of *ta*-C using the Liquids and Amorphous Solids Diffractometer (LAD) at the ISIS pulsed neutron facility of the Rutherford Appleton Laboratory, U.K. This instrument affords high real-space resolution, as scattering vectors with magnitudes Q as high as 500 nm^{-1} can be achieved ($Q=4\pi\sin\theta/\lambda$ for scattering of neutrons with wavelength λ at an angle conventionally denoted by 2θ). A 535 mg specimen of *ta*-C was prepared by deposition on glass substrates, where the poor adhesion of the film allowed its removal from the substrate as a fine powder. Owing to the extended depo-

sition time necessary to produce such a large specimen, a small amount of crystalline graphite from the cathode was unavoidably included in the *ta*-C deposit. However, scattering from powdered graphite measured under identical conditions allowed a successful subtraction of the Bragg peaks from the *ta*-C scattering data. The atomic density of the *ta*-C specimen was calculated using a similar method to that of Gaskell *et al.*[12] from the position of the electron energy-loss plasmon at 30.6 eV, acquired in a scanning transmission electron microscope from regions of the *ta*-C specimen free from graphite contamination.[13] This yielded a value of 1.50×10^{29} m^{-3}. We prefer this method to a macroscopic measurement of the density because the contamination by graphite can be eliminated. A measurement of the H content in the specimen was also made using microcombustion, giving a value close to the error of the measurement (2–3 at. %)[14] The analysis of the scattering data has therefore been conducted assuming the specimen to be pure C.

The scattered intensity was corrected for absorption, multiple, and inelastic scattering using standard procedures.[15] The resulting structure factor $S(Q)$, shown in Fig. 1, is related to the reduced radial distribution function $G(r)$ by

$$G(r)=\frac{2}{\pi}\int_0^\infty Q[S(Q)-1]\sin(Qr)dQ \ . \tag{1}$$

The oscillations in $S(Q)$ were found to be negligible for $Q>250$ nm^{-1}, and the data have therefore been truncated at $Q=245$ nm^{-1}.

The reduced radial distribution function $G(r)$ is shown as the full line in Fig. 2. $G(r)$ is related to the probability of finding an atom in a shell of thickness dr at a distance r from an arbitrary origin. Successive peaks in $G(r)$ correspond to first-, second-, and higher-neighbor atomic distributions. One may model these distributions in terms of a series of Gaussians at distances R, of coordination numbers N and standard deviations σ. Each Gaussian is then convolved with a peak-shape function

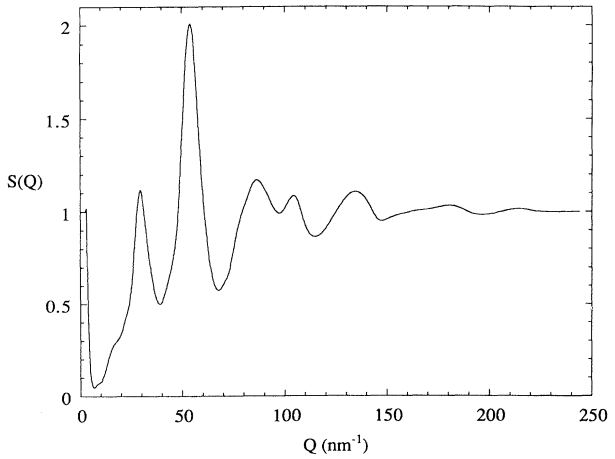

FIG. 1. Structure factor $S(Q)$ for a 535-mg *ta*-C specimen acquired using a pulsed neutron source (ISIS), after subtracting a small contribution from crystalline graphite from the scattering data.

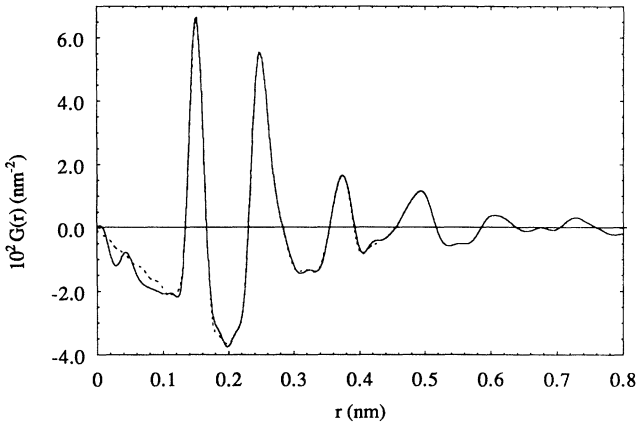

FIG. 2. Reduced radial distribution function $G(r)$ obtained from Fourier inversion of $Q[S(Q)-1]$.

$$P(r)=\frac{Q_{\max}}{\pi}\frac{\sin(Q_{\max}r)}{Q_{\max}r} \tag{2}$$

to include the effects of Q-space termination at $Q_{\max}=245$ nm^{-1}. This fit is shown as the dashed line in Fig. 2, and the corresponding parameters are listed in Table I.

The mean C-C bond length, R_1, is found to be 0.152 nm, close to its value in crystalline diamond, 0.154 nm. The static broadening σ_S due to fluctuations in C-C bond lengths in *ta*-C is estimated from the width of the first peak σ using

$$\sigma_S=[(\sigma)^2-(\sigma_T)^2]^{1/2} \ . \tag{3}$$

Here, the thermal broadening σ_T is given by the width of the first peak in $G(r)$ measured (under identical conditions) from a crystalline diamond specimen (for which $\sigma_S=0$), assuming that thermal broadening is similar for *ta*-C and diamond. This yields $\sigma_S=0.010$ nm, a value that is significantly higher than in *a*-Si and *a*-Ge,[17] presumably due to the presence of both fourfold and threefold C atoms in *ta*-C.

The fraction of fourfold sites can be estimated by fitting the first peak in $G(r)$ using a mixture of C-C distances typical of graphite and diamond. The best fit corresponds to a fraction of 84% fourfold sites, and a coordination number $N_1=3.84$, as compared to the area of

TABLE I. Mean interatomic distances R, standard deviations σ, and coordination numbers N obtained from the fit to the experimental $G(r)$ for *ta*-C.

R (nm)	σ (nm)	N
0.152	0.011	3.90
0.215	0.011	0.24
0.248	0.013	7.66
0.275	0.014	4.37
0.300	0.013	3.06
0.322	0.013	3.52
0.346	0.017	4.60
0.376	0.014	15.00

the first peak, which yields a value of $N_1 = 3.9$. This fraction of tetrahedrally bonded atoms agrees well with values derived from the analysis of C K-edge features in electron energy-loss spectra.[7,8] The result also agrees well with the estimate from the earlier neutron-scattering measurement of *ta*-C,[12] and this is true for all of the parameters in Table I. The fact that similar results are obtained from independent scattering experiments on different specimens strongly suggests that the parameters in Table I are *genuinely* representative of the atomic structure of *ta*-C.

The bond angle θ can be obtained from $\theta = 2\sin^{-1}(R_2/2R_1)$, where R_2 is the position of the major Gaussian component of the second peak (i.e., 0.248 nm). This gives $\theta = 109.3°$, which is close to the tetrahedral value of 109.5°. However, a fraction of the third peak at 0.275 nm may be due to second neighbors, which would imply a slightly higher bond angle. In addition, the minimum between the first and second peaks is found to contain 0.24 atoms, although this value is only marginally significant. Similar findings were reported by Gaskell *et al.*[12]

III. STRUCTURAL MODELING

The parameters in Table I make it clear that the average local structure of *ta*-C is much closer to tetrahedral than trigonal, in particular the position of the first peak in $G(r)$. The coordination number N_1 and the bond angle θ are also consistent with a predominantly tetrahedral network, but the values of these parameters depend on the procedure used to analyze the data—coordination numbers are sensitive to the measured density of the material, and as mentioned above the mean bond angle depends on the fraction of second neighbors assumed to lie within the third peak at 0.275 nm. A reliable description of the second-neighbor distribution requires the use of three-dimensional space-filling models, and it is to this aspect of the analysis that we now turn.

Comparison of neutron-scattering data with three-dimensional models has a dual purpose: first, it allows a more detailed interpretation of features in the experimental data, and second, competing models can be distinguished by the extent of their agreement with experimental data. We first question the extent to which threefold sites are important in modeling $G(r)$ by focusing on the structure of the underlying tetrahedral network, and comparing the experimental scattering data with fully tetrahedral models for *a*-Si and *a*-Ge, and then include models specifically designed to describe the structure of dense *a*-C.

The most widely accepted model for the structure of (defect-free) *a*-Si and *a*-Ge is a network comprising randomly interconnected tetrahedra, such as the model built by Polk and Boudreaux,[16] which gave better agreement with experimental data (for *a*-Ge) than any of the other models available at the time.[17] Recently, a tetrahedral random network with periodic boundary conditions was generated by Wooten and co-workers,[18] who used a bond-switching procedure along with relaxation of the Keating energy[19] to progressively alter the topology of a Si lattice. The resulting tetrahedral networks were in very good agreement with experimental neutron-scattering data for *a*-Ge.[18]

Compared with *a*-Si and *a*-Ge, very few physical models have been built specifically for *a*-C, due in part to the lack of good experimental structural data for the material. The only hand-built models for *a*-C were constructed by Beeman *et al.*[20] who produced three random network models with different proportions of threefold and fourfold sites, and then minimized the energy of each model with the Keating potential. The models were then compared with experimental diffraction data for thermally evaporated *a*-C, and in all cases the agreement with experiment was poor. In addition, Robertson[21] noted that the distribution of threefold sites was unphysical, in that many odd-membered rings of such sites were incorporated into the models, which resulted in a high density of electronic defects states at the Fermi level.

Several computer-generated models for *a*-C have now been reported,[22–31] such as those produced by Tersoff[22] and Kelires[23] via a Monte Carlo algorithm, using an empirical atomic potential due to Tersoff.[22] Low-density models (55–60 % of the diamond density) are found to possess about 10% tetrahedral bonding, with bond lengths and bond angles close to those of graphite, whereas models with a high density (90% of that of diamond) possess proportions of up to 70% fourfold sites, with a corresponding shift in bond lengths and bond angles towards those of diamond. The higher-density models are highly strained, with mean atom energies 0.3 eV higher than those of the predominantly threefold models. Kelires annealed one such model at 1200 K and reported an energy decrease of 0.2 eV/atom, along with a decrease in the percentage of fourfold sites to 27%.[23] Both models were found to contain a high density of electronic states in the gap, due to the absence of an explicit π-bonding term.[24]

Wang and co-workers[25–27] used a molecular-dynamics approach with an empirical tight-binding potential to generate models of both the low-[25] and high-[26,27] density forms of *a*-C, for a periodic cell containing 216 atoms. Calculations by Wang and Ho[27] showed that the presence of an electronic band gap of 2 eV in *ta*-C is consistent with threefold sites clustered in groups of two and four atoms, with both odd numbers and large clusters of threefold sites producing a high density of electronic states at the Fermi level.

Comprehensive simulation studies of *a*-C by Frauenheim and co-workers[28,29] have recently been performed using a local-orbital method within the local-density approximation (LDA). These workers were primarily interested in trends in the structural and electronic properties of *a*-C and *a*-C:H as a function of the proportion of fourfold sites and H concentration. For example, increasing the density of *a*-C models from 2000 kgm^{-3} to 3520 kgm^{-3} produced a variation in the percentage of fourfold sites from 9% to 88%.[29] They carried out a detailed analysis of the electronic structure of the models, and found that increasing the density above 2400 kgm^{-3} led to a competition between the reduction of the π-bonded component and the generation of elec-

tronic defects at the Fermi level. Interestingly, the formation of "weak" σ bonds between three-coordinated atoms was found to partly saturate these defect states at a density of 3000 kgm^{-3}, producing a stable structure with a band gap in the region of 3 eV.[29]

Drabold, Fedders, and Stumm[30] have also simulated dense a-C using molecular dynamics in the local-orbital, local-density approximation, using a 64-atom supercell. They found that the pairing of threefold sites in the model produced a defect-free optical gap of more than 2 eV, in good agreement with experiment.[9,10] In addition, several four-coordinated atoms were found to form so-called "geometrical" defects, consisting of highly strained bonds and angles, which interacted with the three-coordinated defects to minimize the total energy.

The most sophisticated simulation of low-density a-C is due to Galli and co-workers,[31] who used molecular dynamics within a self-consistent LDA to generate a 54-atom model from a cubic diamond supercell, at a fixed density of 2000 kgm^{-3}. The final model consisted of 85% threefold sites, which were distributed in several thick planes cross-linked by fourfold sites.

A. Comparison with experimental data

In this work the structural properties of six models have been calculated: (i) and (ii) The tetrahedral networks of Polk and Boudreaux[16] and Wooten, Winer, and Weaire,[18] rescaled to the C-C bond length in diamond (0.154 nm), referred to as PB and WWW, respectively; (iii) the 356-atom model of Beeman *et al.*,[20] containing 51% fourfold sites, referred to as B356;[32] (iv) a model produced by Wang, Ho, and Chan[26] with 73% fourfold sites, referred to as WH; (v) a 128-atom model generated by Frauenheim and co-workers[28,29] with a density of 3000 kgm^{-3}, referred to as F128; (vi) a 64-atom model produced by Drabold, Fadders, and Stumm,[30] which will be referred to as DFS.

The coordinates of each model have first been used to calculate the reduced radial distribution function $G(r)$. For nonperiodic models, only atoms within a radius $R_{\max}$ of the model center are used in the calculation, where $R_{\max}$ is determined by calculating the density as a function of distance r from the center of the model, and finding the value of r at which the density begins to fall off, owing to the sampling of the space exterior to the model. Following Duffy, Boudreaux, and Polk,[33] the calculated $G(r)$ is then corrected for finite model size by dividing by the function

$$M(r)=1-\frac{3}{4}\left[\frac{r}{R_{\max}}\right]+\frac{1}{16}\left[\frac{r}{R_{\max}}\right]^3. \quad (4)$$

For periodic models, $G(r)$ is calculated for interatomic distances up to half the cubic cell dimension. Each calculated distribution function is then convolved with the peak-shape function (2) corresponding to the $Q_{\max}$ value of 245 nm^{-1} used to produce the experimental $G(r)$.

The models contain varying degrees of static broadening, which in all cases is significantly less than the experimental value of 0.010 nm for the first peak in $G(r)$. Each model $G(r)$ has been convolved with a Gaussian which produces the best agreement between the first peak in $G(r)$ for model and experiment. The standard deviation of this Gaussian is 0.0065 nm for the WH model, 0.0071 nm for the F128 model, 0.0073 nm for the B356 model, 0.0077 for the DFS model, 0.0093 nm for the WWW model, and 0.010 nm for the PB model. The values are highest for the WWW and PB models, as they contain only fourfold sites, but the bond-length distortion in the models with threefold sites is still significantly lower than the experimental value.

Figure 3 shows the comparison between each model and the experimental data of Fig. 2. The atomic densities ρ_0 of the models vary significantly, and some densities are as much as 15% higher than the experimental value of 1.50×10^{29} m^{-3} (see Table II), as shown by the increased slope of $G(r)$ relative to the experimental curve. For the networks with mixed bonding, the position of the first peak in $G(r)$, R_1, depends on the percentage F_4 of fourfold sites. However, a range of values of F_4 produce similar values for R_1 (Table III), as the minimum change in bond length which can be considered significant is 0.001 nm, a variation of about $\pm10\%$ in F_4. This implies that all of the models, with the exception of the tetrahedral models WWW and PB, possess values for R_1—and hence F_4—which are consistent with the experimental $G(r)$.

Comparison of the relative breadths and intensities of second and higher peaks provides a much more stringent test of the validity of a model, as these are related to the topology of the network, and therefore to the procedure by which each model is constructed. In this respect, the usefulness of the 64-atom DFS model is limited, as $G(r)$ can only be calculated to $r=0.38$ nm, which includes only the first and second peaks in $G(r)$. Over the range

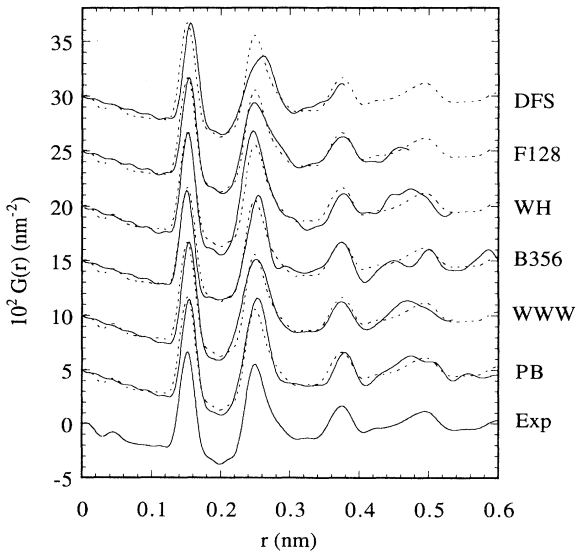

FIG. 3. Comparison of the calculated $G(r)$ for each model with the experimental data (shown as the bottom curve and the dashed curve in all other plots). Some curves have been displaced vertically for clarity.

TABLE II. Structural parameters for each model: Number of atoms N, atomic density ρ_0, fraction of atoms with fourfold coordination F_4, ratio of five- to six-membered rings $P_{5/6}$, mean bond angles $\langle\theta_4\rangle, \langle\theta_3\rangle$ and standard deviations $\sigma(\theta_4)$, $\sigma(\theta_3)$ for fourfold sites and threefold sites, respectively, and Keating energy per atom E_4 for fourfold sites only.

Model	WWW	PB	B356	WH	F128	DFS
N	216	213	191	216	128	64
ρ_0 (10^{29} m^{-3})	1.76	1.70	1.50	1.75	1.50	1.50
F_4	1.00	1.00	0.40	0.73	0.69	84
$P_{5/6}$	0.58	0.46	0.33	0.40	0.75	0.53
$\langle\theta_4\rangle$	109.2	109.2	109.3	109.3	109.2	108.7
$\sigma(\theta_4)$	10.8	8.8	6.7	9.8	10.8	16.0
$\langle\theta_3\rangle$			117.3	118.2	118.4	114.4
$\sigma(\theta_3)$			7.1	10.6	10.1	12.9
E_4 (eV)	0.915	0.573	0.405	0.845	1.05	2.07

0.2–0.4 nm, differences between all the models and experiment can be clearly seen. The peaks in $G(r)$ for the B356 model are narrower than experiment, and a small feature at 0.3 nm is present. In the case of the WH model, the intensity of the second peak is significantly higher than the corresponding peak in the experimental $G(r)$, whereas for the F128 and DFS models the reverse is true, with the second peak in both models now much broader than experiment. Of the two tetrahedral random networks, the WWW model gives slightly better agreement with the experimental $G(r)$ for $0.2 \leq r \leq 0.4$ nm, owing to the broadness of the second peak in $G(r)$. Both random network models can be seen to produce a flat region between the second and third peaks, which results from a continuous distribution of dihedral angles between neighboring tetrahedra. Above 0.4 nm, the agreement with experiment is poor in all cases.

B. Modeling the second-neighbor distribution

A major problem in the structural analysis of *ta*-C is achieving consistency between the first and second coordination numbers, N_1 and N_2. For a fully bonded network with a minimum ring size of 5, N_1 and N_2 are related by the expression $N_2 = N_1(N_1 - 1)$. However, the measured absolute values of N_1 and N_2 are susceptible to systematic errors, as they depend sensitively on parameters such as the atomic density of the material ρ_0. On the other hand, the *ratio* N_2/N_1 is found to remain constant to within about 5% when these parameters are varied, and can therefore be used to obtain an estimate of N_1, denoted N_1^E, which is less likely to contain systematic errors. Thus, $N_1^E = 1 + N_2/N_1$.

The second peak in the experimental $G(r)$ is asymmetric, and is modeled by two Gaussians centered at 0.248 and 0.275 nm. If these are assumed to contain second and third neighbors respectively, then $N_2 = 7.66$, which gives $N_1^E = 3.0$, which is very different from the value of 3.9 obtained from the fit to the first peak in $G(r)$ [neglect of the small angle scattering leads to small errors in the absolute values of $G(r)$, but these are much too small to affect the argument]. This inconsistency between N_1 and N_2 would be reconciled, however, if 3.65 of the 4.37 atoms in the peak at 0.275 nm are assumed to be *second neighbors*, implying an asymmetric second-neighbor distribution.

We test this assumption by fitting the calculated $G(r)$ for each model with Gaussian in exactly the same manner

TABLE III. Peak positions R and coordination numbers N and N^* obtained for each model, where N_1 and N_2 are the mean number of first and second neighbors calculated from the model connectivity, and N_2^* and N_3^* are obtained from a fit to the calculated $G(r)$. $F_{2/3}$ is the fraction of N_3^* corresponding to second neighbors.

Model	WWW	PB	B356	WH	F128	DFS
R_1 (nm)	0.154	0.154	0.151	0.153	0.153	0.153
N_1	4.00	4.00	3.40	3.73	3.69	3.84
R_2 (nm)	0.242	0.252	0.250[a]	0.245	0.246	0.241
N_2^*	6.8	11.9	10.6[a]	10.75	7.64	4.0
R_3 (nm)	0.262	0.262		0.277	0.277	0.267
N_3^*	6.2	1.4		4.85	5.60	7.3
N_2	12.0	12.0	8.08	10.39	10.13	11.06
$F_{2/3}$	0.82	0.07	0.00	0.00	0.44	0.97

[a]The analysis of the B356 model differs in that the asymmetry in the second peak in $G(r)$ is on the low-r side, while the high-r side of the second peak is fitted well without an extra Gaussian. The value of N_2^* for this model is therefore a sum of two Gaussians, and R_2 is the weighted mean of the positions of the Gaussians.

as the experimental data, and extracting the peak positions and coordination numbers for each Gaussian. This procedure then allows a direct comparison between the neighbor distribution of the model and the data in Table I. The fitting has been carried out over the range 0–0.4 nm, and the parameters for the first two peaks in $G(r)$ are given in Table III. In each case, the second peak has been synthesized using two Gaussians with coordination numbers N_2^* and N_3^*. The fraction of N_3^* corresponding to second neighbors, $F_{2/3}$, then determined by direct calculation of the total number of second neighbors N_2 in each model, where $F_{2/3}=(N_2-N_2^*)/N_3^*$ ($F_{2/3}=0$ for $N_2^*>N_2$). The Gaussian fits to the second peak for each model are shown in Fig. 4.

For models PB, B356, and WH, less than 10% of N_3^* consists of second neighbors. Assuming therefore that about 10% of the 4.37 atoms at 0.275 nm are second neighbors yields one estimate of N_2, about 8.5. This gives $N_2/N_1=2.2$ and $N_1^E=3.2$, which is still significantly different from $N_1=3.9$, and probably lies outside the error of the measurement. In addition, a value of $N_1^E=3.2$ implies only 20% fourfold bonding, which is clearly inconsistent with a mean C-C bond length 0.152 nm, a parameter which is *insensitive* to changes in the fitting criteria.

We must therefore assume that the second-neighbor distribution is actually asymmetric, as in the WWW, F128, and DFS models. For these models, N_3^* actually contains 5.2, 2.49, and 7.06 second neighbors respectively, with two roughly similar Gaussians being required to fit the second peak in $G(r)$ for the WWW model. If the ratio of second and third neighbors making up the peak at 0.267 nm for the WWW model is used in conjunction with the experimental values in Table I, then N_2 is found to be 11.3 and N_2/N_1, 2.9, giving $N_1^E=3.9$. This estimate of N_1 is now in good agreement with the value obtained from the fit to the first peak in the experimental $G(r)$. A value of $N_1^E=3.5$ is obtained using the F128 model, which may lie within the bounds of the error in the experimentally measured coordination number.

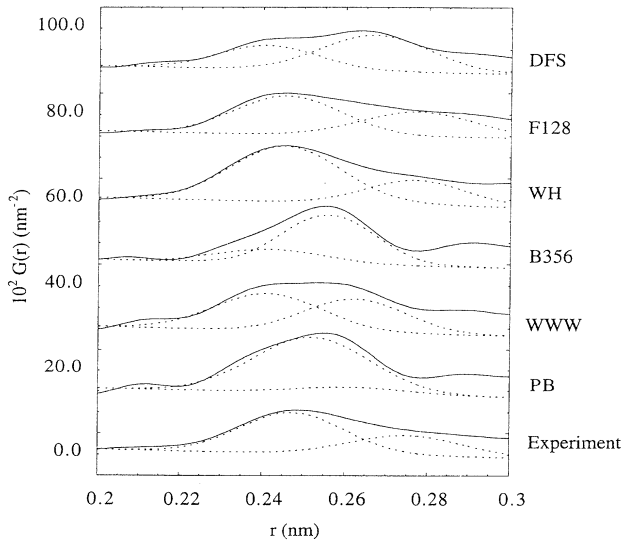

FIG. 4. Comparison of the two Gaussians (dashed curves) used to synthesize the second peak in the experimental $G(r)$ (bottom) and the calculated $G(r)$ for each of the models. Some curves have been displaced vertically for clarity.

These models therefore possess a second-neighbor distribution which *removes* the apparent inconsistency outlined at the beginning of the section. In the case of the DFS model, however, N_3^* is almost twice as large as N_2^*, which is not compatible with the experimental results. While the DFS model gives an accurate representation of electronic structure [i.e., a clean gap of about 2 eV (Ref. 30)], it is likely that this model is too small for a reliable description of atomic structure.

C. Comparison of models

The ratio of five- to six-membered rings per atom $P_{5/6}$ has been calculated using the "shortest path" criterion of Franzblau,[34] and these are listed in Table II. The values of $P_{5/6}$ are roughly similar for the WWW, FB, F128, and WH models, whereas the B356 model contains a higher relative proportion of six-membered rings. In addition, the WWW model contains four four-membered rings, while the DFS model contains five four-membered and four three-membered rings. The presence of these rings contributes to a relatively large spread in bond angles, as discussed below.

Although the mean bond angle for fourfold sites, $\langle\theta_4\rangle$, is broadly similar across all models, its standard deviation $\sigma(\theta_4)$ varies significantly, with the highest and lowest values found for the DFS and B356 models respectively. This gives some indication of the relative angular strain in the models. Another way of characterizing the relative distortion at fourfold sites is to calculate the strain energy density using the Keating parameters for C calculated by Martin,[35] which includes contributions from both bond-length and bond-angle distortion. These values, E_4, are also listed in Table II. For the WWW model at least, it is clear that the agreement with the experimental $G(r)$ over the range 0.2–0.4 nm is a direct result of the high distortion in the model, as reflected in the relatively high strain energy. For the highly strained F128 and DFS models, however, the agreement with experiment over this range is still poor.

While $\langle\theta_4\rangle$ is closer to the tetrahedral value for all models, $\langle\theta_3\rangle$ is always less than the value of 120° found in graphite. This occurs because the threefold sites in the models are generally nonplanar, which may largely be due to the strain imposed by neighboring tetrahedral sites.

IV. MODEL REFINEMENT

A. Refinement without topological changes

Although all of the models possess differences in their short-range structure, i.e., trigonal and/or tetrahedral sites in varying proportions, there are also significant topological differences reflected in the features in $G(r)$ between 0.2 and 0.5 nm, as shown in Fig. 3. It would clear-

ly be useful to examine whether the agreement with the experimental $G(r)$ can be improved without altering the network topology, by making random adjustments to atomic positions subject to a given set of constraints, as implemented in the reverse Monte Carlo (RMC) algorithm.[36] One constraint is of course the agreement between experimental and calculated $G(r)$ or $S(Q)$. The other constraint in many other RMC simulations is the imposition of an excluded volume (hard sphere potential) around each atom, but this can lead to significant bond-length and bond-angle distortion, which is clearly undesirable in covalently bonded networks.

Recent RMC studies of tetrahedral amorphous materials[37]—in which constraints on the coordination number were applied—showed that models with very different coordination numbers were nonetheless dominated by approximately tetrahedral bonding. This is perhaps not surprising given the somewhat arbitrary definition of coordination number, and the fact that any two atoms bonded to a common third atom at the correct distance [i.e., the first peak in $G(r)$] will best fit the experimental $G(r)$ if the angle between them is close to the tetrahedral angle. What needs to be done—and is being attempted here—is to find models which are consistent with both electronic *and* structural data for *ta*-C, which (especially in the former case) requires both that the bonds around each atom are not excessively strained and that threefold sites do not introduce defect states in the gap. The first of these requirements is addressed in this section, and the second in the following section.

The approach used here is to include a simple valence potential,[38,39] containing bond stretching and bond bending terms, in the RMC algorithm as an additional constraint, allowing the procedure to explore local potential-energy minima while sampling the configuration space of the model. This approach ensures that the local geometry around each site is prevented from becoming grossly distorted in order to fit the experimental data. The acceptance of each atomic adjustment is controlled by a Boltzmann expression containing the difference between the energies of the initial and final configurations and an adjustable parameter $k_B T$, where T acts as an effective temperature.

The RMC algorithm has been applied to each model for a time corresponding to 10^6 attempted atomic adjustments, with $k_B T$ being varied from 0.005 eV to 0.05 eV, which is significantly less than the energy required to break bonds. The ratio of accepted to rejected moves was found to be very small, ranging from 1:500 to 1:1500. In general, the local potential minimum occupied by the predominantly tetrahedral models, i.e., WWW, PB, and WH, was found to be both narrow and deep, with the result that improvement in the agreement between calculated and experimental $G(r)$ would have required quite high values of $k_B T$ (>0.2 eV), resulting in significant additional bond-length and bond-angle distortion. This was not attempted, as excessive computational time would then be required to find a new local minimum. Refinement of the DFS model was also not possible without altering the network topology, owing to the presence of three-membered rings.

TABLE IV. Some structural parameters for the RMC-modified models. See Tables I and II for a definition of each parameter.

Model	F128^{RMC}	B356^{RMC}	PB^{RMC}	WWW^{RMC}
F_4	0.69	0.40	0.85	0.85
$P_{5/6}$	0.75	0.33	0.54	0.64
$\langle\theta_4\rangle$	109.2	109.3	109.3	109.2
$\sigma(\theta_4)$	10.7	7.8	7.9	10.3
$\langle\theta_3\rangle$	117.9	117.7	114.4	114.3
$\sigma(\theta_3)$	8.9	6.7	9.5	11.1
E_4 (eV)	0.993	0.556	0.561	0.912
R_1 (nm)	0.153	0.151	0.153	0.153
N_1	3.69	3.40	3.85	3.85
R_2 (nm)	0.248	0.248	0.246	0.245
N_2^*	7.73	7.6	8.75	7.9
R_3 (nm)	0.276	0.276	0.271	0.267
N_3^*	4.27	4.6	4.60	4.5
N_2	10.13	7.91	10.75	11.06
$F_{2/3}$	0.56	0.07	0.43	0.70

In the case of the F128 and B356 models, successful refinement of the model structure was achieved without topological alterations, as evidenced by the absence of any changes in the ring distributions or coordination numbers (Table IV). Agreement with experiment for the F128 model was significantly improved in the range 0.2–0.5 nm with a slight decrease in strain energy, while the B356 model was refined without increasing its energy per atom by more than 0.15 eV. The fits to the experimental $G(r)$ for the B356 and F128 models are shown in Fig. 5, where the RMC-modified models are referred to as B356^{RMC} and F128^{RMC}, respectively. The improvement can be seen by comparing Fig. 5 with Fig. 3.

B. Refinement after bond rearrangements

A more sophisticated technique for modifying networks involves bond rearrangements. Clearly, bond breaking is necessary to introduce threefold sites into the fully tetrahedral WWW and PB models, which possess

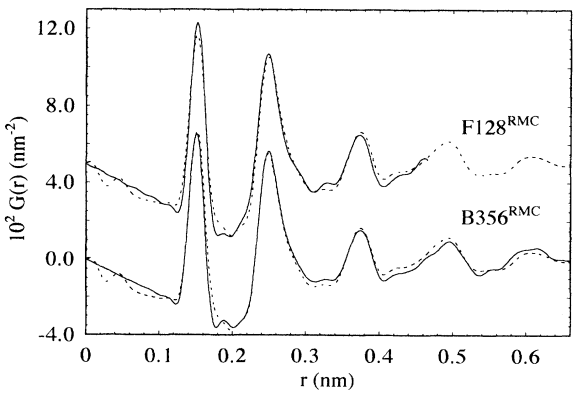

FIG. 5. Comparison of the calculated $G(r)$ for the F128^{RMC} and B356^{RMC} models (solid curves) with the experimental data (dashed curves). Some curves have been displaced vertically for clarity.

discrepancies between experimental and calculated $G(r)$ below 0.2 nm. However, breaking bonds at random would produce large numbers of isolated threefold sites, i.e., dangling bonds, which is ruled out by the practically defect-free nature of the gap.[9] The method chosen here is therefore to produce *pairs* of threefold sites by breaking alternate bonds around an even-membered ring. In principle, this procedure can lower both the mean coordination and bond length, and introduce the bond-length distortion required to fit the first peak in the experimental $G(r)$.

However, as each chain of threefold sites is anchored at both ends by tetrahedra, it is not free to rotate in order to maximize the π interaction along the chain, and therefore converting two neighboring tetrahedra with a large dihedral angle to a pair of trigonal sites would result in a small degree of overlap, and hence a significant dangling bond character. This effect was pointed out by Lee *et al.*[24] who calculated the local density of states for several triply-bonded configurations embedded in the WWW model, in which dihedral angle disorder between neighboring threefold sites resulted in a reduced π-π^* splitting. Similar trends were found by Stephan *et al.*[29] In this work, therefore, we have maximized the π overlap between the resulting threefold sites by selecting rings comprising tetrahedra with dihedral angles as close to zero (eclipsed configuration) as possible. This choice is made more justifiable on the grounds that eclipsed tetrahedra are energetically less favorable in the crystalline phase than staggered tetrahedra, thus reducing the cost in energy of breaking bonds to form threefold sites.

A percentage of threefold sites varying from 10% to 20% has therefore been introduced into both the WWW and PB models in the manner described above, using the CERIUS suite of three-dimensional molecular modeling routines produced by Molecular Simulations, Inc. and the resulting networks relaxed using a simple valence potential,[38,39] which approximately describes the strong σ bonding in the networks, but neglects the weaker π bonding between adjacent threefold sites. For both the WWW and PB models, introducing 15% threefold sites was found to give the best agreement with the first peak in the experimental $G(r)$. The RMC algorithm was then applied to each model for 10^6 generated moves, with no significant energy increase for either model.

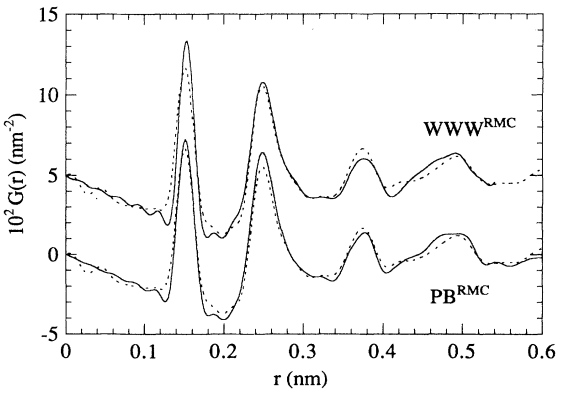

FIG. 6. Comparison of the calculated $G(r)$ for the WWW^{RMC} and PB^{RMC} models (solid curves) with the experimental data (dashed curves). Some curves have been displaced vertically for clarity.

Figure 6 shows the comparison between the calculated and experimental $G(r)$ after RMC refinement, and the structural parameters of the RMC-modified models are listed in Table IV. Small changes can be seen in most parameters, particularly F_4. The low values of $\langle \theta_3 \rangle$ result from a significant out-of-plane distortion in the threefold sites, which was difficult to avoid owing to the high density of the models. Reducing the density would have created a considerable number of broken bonds, which is beyond the scope of the potential used in this work.

It is clear from Fig. 6 that the agreement with experiment has now been improved over the entire range covered by the models, in particular the second peak in $G(r)$. For the modified models, $G(r)$ has been broadened with a Gaussian of width 0.004 nm, corresponding to the measured thermal broadening σ_T, that is, no artificial broadening has been used. The static distortion in both models is still slightly lower than experiment, and in this respect the F128^{RMC} model gives better overall agreement with the experimental $G(r)$ than either the WWW or PB model. The energy density of the models is high, with the F128^{RMC} model about 0.08 eV and 0.43 eV higher than the WWW^{RMC} and PB^{RMC} models, respectively, and a relatively high degree of strain energy appears to be an essential ingredient in the structural modeling of *ta*-C.

Although the threefold sites in the WWW^{RMC} and PB^{RMC} models have been introduced in such a way as to maximize the π overlap, and hence minimize the density of midgap states, the success of the method needs to be tested by performing a relaxation of the modified network with a realistic electronic potential, and this is presently being carried out on the WWW^{RMC} model.[40]

V. CONCLUSIONS

The neutron structure factor of *ta*-C has been measured to high values of Q, and is in good agreement with earlier data measured on a much smaller specimen. While the reliability of the data is now improved, the partial crystallinity of the specimen imposes some limitations, so that coordination numbers are subject to some uncertainty. The experimental data once again suggests that the material is mostly tetrahedrally bonded, and the difficulty remains in reconciling the first and second coordination numbers. The two quantities agree if it can be assumed that the second peak in $G(r)$ contains only 16% of third neighbors.

Several models constructed specifically for high-density *a*-C have been compared with the experimental $G(r)$, along with models designed for other tetrahedral amorphous solids—Si and Ge. It is shown that while reasonable agreement is obtained for some models, none give an adequate level of agreement. Features in $G(r)$ are poorly reproduced, such as the breadth of the first-neighbor distribution. In addition, the second-neighbor distribution in most models is narrower than experiment suggests. In

the case of the WWW and F128 models, however, the asymmetry in the second-neighbor distribution removes the inconsistency between the first and second coordination numbers. The strain energy density for *ta*-C has not been measured so that it is not possible to compare this quantity with model data, but the wide range of values found indicates that only some models can be correct.

Attempts to refine the F128 and B356 models using RMC have proved successful without the need for topological alterations, suggesting that the topology of the models is consistent with the experimental $G(r)$, although only the F128 model possesses a physically realistic distribution of threefold sites. In most cases, application of RMC produces no significant improvement, probably because improvements to the quality of the fit to the neutron data would require a move to a region of configuration space involving breaking bonds and modifying the topology, and this has been deliberately prevented.

Introduction of pairs of threefold sites into the purely tetrahedral models followed by RMC gives considerable improvements to the agreement with the experimental $G(r)$, particularly in the second peak. The breadth of the first peak is now adequately reproduced without the need for additional (arbitrary) broadening terms. It therefore seems that predominantly tetrahedral models with considerable elastic strain incorporating about 15% three-coordinated C atoms are required to adequately model the structural properties revealed in the neutron-scattering data. While the RMC-modified F128 model provides better overall agreement with experiment, its strain energy density is higher than either of the tetrahedral models, and whether such strain will prove to be consistent with the heat of crystallization is an interesting question and must await experimental determination of the latter.

ACKNOWLEDGMENTS

The authors would like to thank Dr. D. R. McKenzie for providing the *ta*-C specimen used in this work, and W. S. Howells for invaluable assistance during the neutron-scattering measurements. We would also like to thank Professor F. Wooten, Professor D. Beeman, Dr. C. Z. Wang, Dr. Th. Frauenheim, and Dr. D. A. Drabold for the use of the WWW, B356, WH, F128, and DFS models, respectively, and Dr. D. S. Franzblau for use of the program for calculating ring statistics. We have also benefited from discussions with Dr. D. A. Drabold, Dr. G. A. J. Amaratunga, and Dr. C. A. Davis. One of us (K.W.R.G.) acknowledges the generous financial support of the Royal 1851 Commission for work done at the Cavendish Laboratory, Cambridge, U.K.

*Present address: School of Physics, University of East Anglia, Norwich NR4 7TJ. Electronic address: k.gilkes@uea.ac.uk

[1]I. I. Aksenov, V. A. Belous, V. G. Padalka, and V. M. Khoroshikh, Sov. J. Plasma Phys. **4**, 425 (1978).

[2]R. Lossy, D. L. Pappas, R. A. Roy, and J. J. Cuomo, Appl. Phys. Lett. **61**, 171 (1992).

[3]Y. Lifshitz, S. R. Kasi, and J. W. Rabalais, Phys. Rev. Lett. **68**, 620 (1989).

[4]J. Robertson, Prog. Solid State Chem. **21**, 199 (1991); Philos. Trans. R. Soc. A **342**, 277 (1993); Surf. Coat. Technol. **50**, 185 (1992).

[5]D. R. McKenzie, D. Muller, and B. A. Pailthorpe, Phys. Rev. Lett. **67**, 773 (1991).

[6]D. R. McKenzie *et al.*, Diam. Relat. Mater. **3**, 353 (1994).

[7]S. D. Berger, D. R. McKenzie, and P. J. Martin, Philos. Mag. Lett. **57**, 285 (1988).

[8]P. Fallon, V. S. Veerasamy, C. A. Davis, J. Robertson, G. A. J. Amaratunga, W. I. Milne, and J. Koskinen, Phys. Rev. B **48**, 4777 (1993).

[9]V. S. Veerasamy, G. A. J. Amaratunga, C. A. Davis, W. I. Milne, P. Hewitt, and M. Weiler, Solid-State Electron. **37**, 319 (1994).

[10]V. S. Veerasamy, J. Yuan, G. A. J. Amaratunga, W. I. Milne, K. W. R. Gilkes, W. Weiler, and L. M. Brown, Phys. Rev. B **48**, 17 954 (1993).

[11]V. S. Veerasamy, G. A. J. Amaratunga, C. A. Davis, A. E. Timbs, W. I. Milne, and D. R. McKenzie, J. Phys. Condens. Matter **5**, L169 (1993).

[12]P. H. Gaskell, A. Saeed, P. Chieux, and D. R. McKenzie, Phys. Rev. Lett. **67**, 1286 (1991); Philos. Mag. B **66**, 155 (1992).

[13]K. W. R. Gilkes and P. J. Fallon (unpublished).

[14]C. T. Pillinger (private communication).

[15]M. A. Howe, R. L. McGreevy, and W. S. Howells, J. Phys. Condens. Matter **1**, 3433 (1989).

[16]D. E. Polk and D. S. Boudreaux, Phys. Rev. Lett. **31**, 92 (1973).

[17]G. Etherington, A. C. Wright, J. T. Wenzel, J. C. Dore, J. H. Clarke, and R. N. Sinclair, J. Non-Cryst. Solids **48**, 265 (1982).

[18]F. Wooten and D. Weaire, J. Non-Cryst. Solids **64**, 325 (1984); F. Wooten, K. Winer, and D. Weaire, Phys. Rev. Lett. **54**, 1392 (1985).

[19]P. N. Keating, Phys. Rev. **145**, 637 (1966).

[20]D. Beeman, J. Silverman, R. Lynds, and M. R. Anderson, Phys. Rev. B **30**, 870 (1984).

[21]J. Robertson, Adv. Phys. **35**, 317 (1986).

[22]J. Tersoff, Phys. Rev. Lett. **61**, 2879 (1988).

[23]P. C. Kelires, Phys. Rev. Lett. **68**, 1854 (1992); Phys. Rev. B **47**, 1829 (1993).

[24]C. H. Lee, W. R. L. Lambrecht, B. Segall, P. C. Kelires, Th. Frauenheim, and U. Stephan, Phys. Rev. B **49**, 11 448 (1994).

[25]C. Z. Wang, K. M. Ho, and C. T. Chan, Phys. Rev. Lett. **70**, 611 (1993).

[26]C. Z. Wang, K. M. Ho, and C. T. Chan, Phys. Rev. Lett. **71**, 1184 (1993).

[27]C. Z. Wang and K. M. Ho, J. Phys. Condens. Matter **6**, L239 (1994).

[28]Th. Frauenheim, P. Blaudeck, U. Stephan, and G. Jungnickel, Phys. Rev. B **48**, 4823 (1993).
[29]U. Stephan, Th. Frauenheim, P. Blaudeck, and G. Jungnickel, Phys. Rev. B **49**, 1489 (1994).
[30]D. A. Drabold, P. A. Fedders, and P. Stumm, Phys. Rev. B **49**, 16 416 (1994).
[31]G. Galli, R. M. Martin, R. Car, and M. Parrinello, Phys. Rev. Lett. **62**, 555 (1989); Phys. Rev. B **42**, 7470 (1990).
[32]Although Beeman's models possess odd-membered rings of threefold sites, and are therefore not consistent with electronic data for *ta*-C, we have nonetheless included the 356-atom model in order to investigate the topology of the network, as this model is the only *hand-built* random network containing both threefold and fourfold sites.
[33]M. G. Duffy, D. S. Boudreaux, and D. E. Polk, J. Non-Cryst. Solids **15**, 435 (1974).
[34]D. S. Franzblau, Phys. Rev. B **44**, 4925 (1991).
[35]R. M. Martin, Phys. Rev. B **1**, 4005 (1970).
[36]R. L. McGreevy and L. Pusztai, Mol. Sim. **1**, 359 (1988).
[37]O. Gereben and L. Pusztai, Phys. Rev. B **50**, 14 136 (1994).
[38]N. Tomassini, A. A. Bonapasta, A. Lapiccirella, K. W. Lodge, and S. L. Altmann, J. Non-Cryst. Solids **93**, 241 (1987).
[39]S. Lifson and A. Warshel, J. Chem. Phys. **49**, 5116 (1968).
[40]D. A. Drabold and K. W. R. Gilkes (unpublished).